 CMC, vol.21, no.3, pp.187-208, 2011

Hybrid Finite Element Method Based on Novel General Solutions for Helmholtz-Type Problems

Zhuo-Jia Fu[1,2], Wen Chen[1] and Qing-Hua Qin[2,3]

Abstract: This paper presents a hybrid finite element model (FEM) with a new type of general solution as interior trial functions, named as HGS-FEM. A variational functional corresponding to the proposed general solution is then constructed for deriving the element stiffness matrix of the proposed element model and the corresponding existence of extremum is verified. Then the assumed intra-element potential field is constructed by a linear combination of novel general solutions at the points on the element boundary under consideration. Furthermore, the independent frame field is introduced to guarantee the intra-element continuity. The present scheme inherits the advantages of hybrid Trefftz FEM (HT-FEM) over the conventional FEM and BEM, and avoids the difficulty in choosing appropriate terms of Trefftz functions in HT-FEM and also removing the troublesome for determining fictitious boundary in hybrid fundamental solution-based FEM (HFS-FEM). The efficiency and accuracy of the proposed model are assessed through several numerical examples.

Keywords: Hybrid finite element, general solution, Helmholtz-type problem, nonlinear functionally graded material

1 Introduction

Hybrid finite element method (HFEM) proposed by Pian [Pian (1964); Pian and Tong (1969)] is a robust finite element method, which is based on Hellinger-Reissner variational formulation and the assumed stress fields satisfying the equilibrium equations. In contrast to conventional FEM, HFEM [Pian (1995)] has greater flexibility in obtaining accurate stress distribution, and it employs both assumed

[1] Center for Numerical Simulation Software in Engineering and Sciences, Department of Engineering Mechanics, Hohai University, Nanjing, Jiangsu, P.R.China
[2] School of Engineering, Building 32, Australian National University, Canberra, ACT 0200, Australia
[3] Corresponding author. E-mail: qinghua.qin@anu.edu.au.

displacement and stress polynomials as trial functions to avoid choosing the high-order polynomials. In virtue of its merits, HFEM was applied to various elasticity and structural mechanics problems [Atluri (1971), (1973); Atluri et al. (1975); Pian (1983); Tong et al. (1973); Ying and Atluri (1983)]. Whereafter hybrid crack elements [Atluri et al. (1978); Piltner (1985); Tong (1977); Xiao and Karihaloo (2007)] have been formulated to deal with the region around the crack in fracture elasticity problems. In developing special crack elements, they employ truncated asymptotic crack tip displacement and stress expansions as trial functions, which satisfy all governing equations in advance.

On the other hand, the HT-FEM, introduced in 1977 [Jirousek and Leon (1977)], has been considerably improved and has now become a highly efficient and well established computational tool in the solution of various engineering problems [Qin (1994), (2003a), (2003b)]. Unlike the conventional FEM, HT-FEM is based on a hybrid method which includes imposing intra-element continuity to link up a non-conforming internal field with the inter-element frame field [Qin (2000)]. Such intra-element fields are chosen as suitable T-complete functions so as to *a priori* satisfy the governing equation of the problem under consideration. It should be mentioned that, unlike hybrid crack elements, in HT-FEM the trial functions satisfy all governing equations in advance at element level. Moreover, HT-FEM combines the advantages of Hybrid FEM and boundary element method, its main advantages are: 1) it only needs numerical integration along the element boundaries, which enables arbitrary polygonal or even curve-sided shapes to be generated, 2) it permits great liberty in element geometry and provides the possibility of accurate performance without requiring annoying mesh adjustment to various local effects due to loading and/or geometry changes [Dhanasekar et al. (2006)].

However, the terms of Trefftz functions should be carefully chosen in obtaining desired results [Qin (2000)]. Moreover, it is difficult to derive Trefftz functions for some practical engineering problems. Recently, Wang and Qin [Wang and Qin (2010), (2009)] developed a hybrid finite element method based on the fundamental solution (HFS-FEM), which overcomes the drawback of HT-FEM and uses a linear combination of fundamental solutions at points on the fictitious boundary outside the elemental domain under consideration to construct the intra-element field. Nevertheless, selecting the appropriate fictitious boundary becomes a new headache in the HFS-FEM as in the method of fundamental solution [Fairweather and Karageorghis (1998); Wang and Qin (2006)], which has a significant effect on the numerical accuracy.

This paper follows the works of HTFEM and HFS-FEM. To remove the drawback of HT-FEM and HFS-FEM mentioned above, a novel type of nonsingular general solutions [Chen et al. (2010); Chen et al. (2005)] is firstly applied to hybrid finite element model (FEM), named as HGS-FEM, which replaces the singular fundamental solutions by the nonsingular general solutions as the interior trial functions and thus enables to place the source points on the element boundary under consideration. The independent frame field is defined along the element boundary to guarantee the intra-element continuity which is the same as that of HFS-FEM. Finally, a variational functional is employed to construct the final stiffness equation and link the boundary frame field with intra-element field. Similar to the HFS-FEM, the proposed HGS-FEM retains all advantages of HT-FEM and removes the difficulty in choosing appropriate terms of Trefftz functions. It is should be mentioned that the nonsingular general solution has one term only, rather than many terms of Trefftz functions in HT-FEM, which makes the corresponding derivation simple. Further, the proposed HGS-FEM avoids determining the position of fictitious boundary, which is required in the HFS-FEM. In addition, it should be pointed out that, in contrast to boundary element method (BEM) [Qin (1993); Sladek and Sladek (1998)], the present approach removes the weakness of dealing with singular or hyper-singular integrals in the BEM.

A brief outline on the structure of paper is as follows: Section 2 presents a detailed derivation of the proposed HGS-FE model. In Section 3, three typical examples are considered to demonstrate the numerical efficiency and accuracy of the proposed HGS-FEM in comparison with the HFS-FEM and the boundary knot method (BKM) [Fu et al. (2011)]. Finally, Section 4 presents some conclusions and potential extensions of the proposed model.

2 HGS Finite element model

2.1 Basic equation of Helmholtz equation

For a practical engineering problem, its physical behavior is generally governed by the following field equations:

$$Ru + \bar{b} = 0 \text{ (in } \Omega\text{, governing equation)} \tag{1}$$

subjected to the boundary conditions

$$u = \bar{u} \text{ (on } \Gamma_u\text{, essential boundary condition)} \tag{2a}$$

$$t = Bu = \bar{t} \text{ (on } \Gamma_t\text{, natural boundary condition)} \tag{2b}$$

where R and B are differential operators, $\bar{b}$ denotes inner heat source.

As an illustration of the proposed HGS-FEM, let us consider two-dimensional isotropic Helmholtz problem in the absence of inner sources ($\bar{b} = 0$), where $R = \Delta + \lambda^2$ and $B = \frac{\partial}{\partial x_1} n_{x_1} + \frac{\partial}{\partial x_2} n_{x_2}$, in which Δ is the Laplace operator, λ denotes wave number, u,t represent the potential and flux, $\bar{u},\bar{t}$ are the corresponding prescribed functions, and (n_{x_1},n_{x_2}) the outward unit normal vector at natural boundary Γ_t.

2.2 Assumed fields

In performing HGS-FE analysis, the whole domain Ω is divided into a number of elements. For a particular element, say element e, occupying a sub-domain Ω_e with the element boundary Γ_e, two groups of independent fields are assumed in the following way:

1) A non-conforming intra-element field is defined by

$$u_e(\mathbf{x}) = \sum_{j=1}^{Ns} N_e(\mathbf{x},y_j)\,c_{ej} = \mathbf{N}_e(\mathbf{x})\,\mathbf{c}_e \;\forall\mathbf{x}\in\Omega_e, \mathrm{y}\in\partial\Omega_e \tag{3}$$

where $\mathbf{c}_e$ stands for unknown parameters and Ns represents the number of source points located on the element boundary. $N_e(\mathbf{x},y_j)$ is the nonsingular general solutions of two-dimensional isotropic Helmholtz problem [Chen and Tanaka (2002)]:

$$N_e(\mathrm{x},\mathrm{y}) = \frac{1}{2\pi}J_0(\lambda r)$$

in which J_0 denotes the zero-order Bessel function of first kind, and r is the Euclidian distance between the collocation point $\{\mathrm{x}\}$ and source point $\{y\}$. Some useful nonsingular general solutions [Chen et al. (2010); Chen et al. (2005)] are listed in Appendix 1. Unlike in the HFS-FEM, the proposed HGS-FEM places the source points coinciding with the collocation points on the element boundary, usually on the same set of boundary nodes displayed in Fig. 1. Additionally, it should be mentioned that the assumed intra-element temperature field is defined in a local reference system $\mathbf{x}=(x_1,x_2)$ whose axis remains parallel to the axis of the global reference system $\mathbf{X}=(X_1,X_2)$ (see Fig. 1).

The corresponding outward normal derivative of u_e on Γ_e is defined by

$$t_e = \sum_{i,j=1}^{2}\frac{\partial u_e}{\partial x_j}n_{x_i} = \mathrm{Q}_e\mathrm{c}_e \tag{4}$$

where

$$\mathbf{Q}_e = \sum_{i,j=1}^{2}\frac{\partial \mathbf{N}_e}{\partial x_j}n_{x_i} = \mathbf{A}\mathbf{T}_e \tag{5}$$

with

$$\mathbf{A} = \begin{bmatrix} n_1 & n_2 \end{bmatrix}, \quad \mathbf{T}_e = \begin{bmatrix} \frac{\partial \mathbf{N}_e}{\partial x_1} & \frac{\partial \mathbf{N}_e}{\partial x_2} \end{bmatrix}^{\mathrm{T}} \tag{6}$$

The undetermined coefficients $\mathbf{c}$, here, may be calculated in many different ways (variational approach, least square, etc.) that enable the prescribed boundary conditions and the inter-element continuity to be approximately fulfilled. The simplest way to enforce the inter-element continuity conditions

$$u_e = u_f \ on \ \Gamma_e \cap \Gamma_f \text{ conformity} \tag{7a}$$

$$t_e + t_f = 0 \ on \ \Gamma_e \cap \Gamma_f \text{ reciprocity} \tag{7b}$$

and to express the unknown coefficients $\mathbf{c}$ in terms of conveniently chosen nodal parameters is a hybrid procedure based on using a frame function representing an independent temperature $\tilde{u}$. So the second independent temperature field should be introduced in the following way.

2) An auxiliary exactly and minimally conforming frame field

$$\tilde{u}_e(\mathbf{x}) = \tilde{\mathbf{N}}_e(\mathbf{x})\,\mathbf{d}_e, \ \mathbf{x} \in \Gamma_e \tag{8}$$

is independently assumed along the element boundary Γ_e in terms of nodal degrees of freedom (DOF) $\mathbf{d}_e$, where $\tilde{\mathbf{N}}_e$ represents the conventional finite element interpolating functions. The frame field on any side with Nf nodes of a particular element can be given in the form

$$\tilde{u} = \sum_{i=1}^{Nf} \tilde{N}_i(\xi)\, u_i \tag{9}$$

where $\tilde{N}_i(\xi)$ denotes shape functions in terms of natural coordinate ξ. Making use of the properties of the shape functions for a one-dimensional line element [Qin and Wang (2009)]:

$$\tilde{N}_i(\xi_i) = 1$$

$$\tilde{N}_j(\xi_i) = 0 \ for \ i \neq j$$

$$\sum_{i=1}^{Nf} \tilde{N}_i(\xi) = 1$$

a series of shape functions with different nodes can be constructed as follows:

(1) shape function of an element edge with 2 nodes

$$\xi = \{-1, 1\}$$

$$\tilde{N}_1(\xi) = \frac{1-\xi}{2},$$

$$\tilde{N}_2(\xi) = \frac{1+\xi}{2}$$

(2) shape function of an element edge with 3 nodes

$$\xi = \{-1, 0, 1\}$$

$$\tilde{N}_1(\xi) = -\frac{\xi(1-\xi)}{2},$$

$$\tilde{N}_2(\xi) = 1-\xi^2,$$

$$\tilde{N}_3(\xi) = \frac{\xi(1+\xi)}{2}$$

(3) shape function of an element edge with 4 nodes

$$\xi = \left\{-1, -\frac{1}{3}, \frac{1}{3}, 1\right\}$$

$$\tilde{N}_1(\xi) = \frac{1}{16}(1-\xi)\left(-10+9\left(\xi^2+1\right)\right),$$

$$\tilde{N}_2(\xi) = \frac{9}{16}\left(1-\xi^2\right)(1-3\xi),$$

$$\tilde{N}_3(\xi) = \frac{9}{16}\left(1-\xi^2\right)(1+3\xi),$$

$$\tilde{N}_4(\xi) = \frac{1}{16}(1+\xi)\left(-10+9\left(\xi^2+1\right)\right).$$

2.3 Modified variational principle

The HGS FE formulation for Helmholtz problem can be established by the variational approach [Qin (2005); Qin and Wang (2009)]. The approach is based mainly on a modified variational principle. The terminology "modified principle" refers here to the use of conventional potential functional and some modified terms for the construction of a special variational principle. The reason for employing the modified terms is that satisfaction of continuity displacement and flux between elements (Eq. (7)) and natural boundary conditions cannot be guaranteed in the HGS-FEM due to the use of general solutions as the intra-element function within an element. Following the procedure given in [Qin and Wang (2009)], the functional corresponding to the problem defined in Eqs. (1) and (2) is constructed as

$$\Pi_m = \sum_e \Pi_{me} \tag{10}$$

with

$$\Pi_{me} = \frac{1}{2}\int_{\Omega_e} \left(u_{,i}u_{,i} - \lambda^2 u^2\right) \mathrm{d}\Omega - \int_{\Gamma_{te}} \bar{t}\tilde{u}\mathrm{d}\Gamma + \int_{\Gamma_e} t\left(\tilde{u} - u\right)\mathrm{d}\Gamma \tag{11}$$

It should be mentioned that in functional (11), the governing equation (1) is satisfied, *a priori*, due to the use of general solutions in the HGS FE model. The boundary Γ_e of a particular element consists of the following parts:

$$\Gamma_e = \Gamma_{ue} \cup \Gamma_{te} \cup \Gamma_{Ie} \text{ and } \Gamma_{ue} \cap \Gamma_{te} = \Gamma_{te} \cap \Gamma_{Ie} = \Gamma_{ue} \cap \Gamma_{Ie} = \emptyset \tag{12}$$

where Γ_{Ie} represents the intra-element boundary of the element 'e'.

Next we prove that the stationary condition of the functional (10) leads to the governing equation (1), boundary conditions (2) and continuity conditions (7). The first-order variational of the functional (11) yields

$$\begin{aligned}\delta\Pi_{me} = &\int_{\Omega_e} \left(u_{,i}\delta u_{,i} - \lambda^2 u\delta u\right)\mathrm{d}\Omega - \int_{\Gamma_{te}} \bar{t}\delta\tilde{u}\mathrm{d}\Gamma \\ &+ \int_{\Gamma_e} \delta t\left(\tilde{u} - u\right)\mathrm{d}\Gamma + \int_{\Gamma_e} t\left(\delta\tilde{u} - \delta u\right)\mathrm{d}\Gamma\end{aligned} \tag{13}$$

By using the divergence theorem

$$\int_{\Omega} \left(f_{,i}h_{,i} + h\nabla^2 f\right)\mathrm{d}\Omega = \int_{\Gamma} hf_{,i}n_i\mathrm{d}\Gamma \tag{14}$$

for any smooth functions f and h in the solution domain, functional (13) can be expressed as

$$\begin{aligned}\delta\Pi_{me} = &-\int_{\Omega_e}\left(u_{,ii}+\lambda^2 u\right)\delta u \mathrm{d}\Omega - \int_{\Gamma_{te}}\left(\bar{t}-t\right)\delta\tilde{u}\mathrm{d}\Gamma \\ &+\int_{\Gamma_e}\delta t\left(\tilde{u}-u\right)\mathrm{d}\Gamma + \int_{\Gamma_{Ie}} t\delta\tilde{u}\mathrm{d}\Gamma + \int_{\Gamma_{ue}} t\delta\tilde{u}\mathrm{d}\Gamma\end{aligned} \tag{15}$$

For the displacement-based method, the potential conformity is satisfied in advance, that is

$$\begin{aligned}&\delta\tilde{u} = \delta\bar{u} = 0 \ on\ \Gamma_{ue}\ \left(\tilde{u}=\bar{u}\right) \\ &\delta\tilde{u}^e = \delta\tilde{u}^f \ on\ \Gamma_{Ief}\ \left(\tilde{u}^e=\tilde{u}^f\right)\end{aligned} \tag{16}$$

Then, Eq. (15) can be rewritten as

$$\begin{aligned}\delta\Pi_{me} = &-\int_{\Omega_e}\left(u_{,ii}+\lambda^2 u\right)\delta u \mathrm{d}\Omega - \int_{\Gamma_{te}}\left(\bar{t}-t\right)\delta\tilde{u}\mathrm{d}\Gamma \\ &+\int_{\Gamma_e}\delta t\left(\tilde{u}-u\right)\mathrm{d}\Gamma + \int_{\Gamma_{Ie}} t\delta\tilde{u}\mathrm{d}\Gamma\end{aligned} \tag{17}$$

from which the governing equation (1) and boundary conditions (2) can be obtained using the stationary condition $\delta\Pi_{me}=0$

$$\left(\Delta+\lambda^2\right)u = 0,\ x\in\Omega \tag{18}$$

$$u = \bar{u},\ x\in\Gamma_u \tag{19a}$$

$$t = \bar{t}, x\in\Gamma_t \tag{19b}$$

We can produce the field continuity requirement Eq. (7) in the following way. When assembling elements 'e' and 'f', we have

$$\begin{aligned}\delta\Pi_{m(e+f)} = &-\int_{\Omega_{e+f}}\left(u_{,ii}+\lambda^2 u\right)\delta\tilde{u}\mathrm{d}\Omega - \int_{\Gamma_{te+tf}}\left(\bar{t}-t\right)\delta\tilde{u}\mathrm{d}\Gamma \\ &+\int_{\Gamma_e}\delta t\left(\tilde{u}-u\right)\mathrm{d}\Gamma + \int_{\Gamma_f}\delta t\left(\tilde{u}-u\right)\mathrm{d}\Gamma + \int_{\Gamma_{Ief}} t\delta\tilde{u}^{ef}\mathrm{d}\Gamma + \cdots\end{aligned} \tag{20}$$

From which the vanishing variation of $\delta\Pi_{m(e+f)}$ leads to the reciprocity condition (7b) $t_e+t_f=0$ on the intra-element boundary Γ_{Ief}.

Theorem: existence of extremum

To prove the existence of extremum of the above variational functional, let us give a proposition first.

Proposition: Suppose the expression

$$\Lambda = \int_{\Gamma_t} \delta t \delta \tilde{u} \mathrm{d}\Gamma + \sum_e \left(\int_{\Gamma_e} \delta t_e \left(\delta \tilde{u}_e - \delta u_e \right) \mathrm{d}\Gamma + \int_{\Gamma_{Ie}} \delta t_e \delta \tilde{u}_e \mathrm{d}\Gamma \right) \tag{21}$$

is uniformly positive (or negative) in the neighborhood of $\{u\}^0$, where the displacement $\{u\}^0$ has such a value that $\Pi_m \left(\{u\}^0 \right) = \Pi_m^0$, and in which Π_m^0 denotes the stationary value of Π_m, namely,

$$\Pi_m \geq \Pi_m^0 \text{ or } \Pi_m \leq \Pi_m^0 \tag{22}$$

where the following relationship has been employed

$$\{\tilde{u}\}_e = \{\tilde{u}\}_f \ on\ \Gamma_e \cap \Gamma_f \tag{23}$$

The expression (23) is due to the definition in Eq. (7a). This proposition can be proved by way of "second variational approach" [Simpson and Spector (1987)]. Therefore, by performing variation of $\delta\Pi_m$ and using the above-mentioned proposition, we obtain

$$\delta^2 \Pi_m = \int_{\Gamma_t} \delta t \delta \tilde{u} \mathrm{d}\Gamma + \sum_e \left(\int_{\Gamma_e} \delta t_e \left(\delta \tilde{u}_e - \delta u_e \right) \mathrm{d}\Gamma + \int_{\Gamma_{Ie}} \delta t_e \delta \tilde{u}_e \mathrm{d}\Gamma \right) = \Lambda \tag{24}$$

In other words, $\delta^2\Pi_m$ is uniformly positive (or negative). Thus it has been proved from the sufficient condition of a local extreme existence of a functional. This concludes the proof.

2.4 Generation of the element stiffness equation

The above modified variational approach links the intra-element field with boundary frame field and then generates the element stiffness equation below. Applying the divergence theorem again to the functional (11), we have the final functional for the HGS-FE model

$$\Pi_{me} = -\frac{1}{2} \int_{\Gamma_e} t u \mathrm{d}\Gamma - \int_{\Gamma_{te}} \bar{t} \tilde{u} \mathrm{d}\Gamma + \int_{\Gamma_e} t \tilde{u} \mathrm{d}\Gamma \tag{25}$$

Substituting Eqs. (3), (4) and (8) into the functional (25) yields

$$\Pi_e = -\frac{1}{2} \mathbf{c}_e^{\mathrm{T}} \mathbf{H}_e \mathbf{c}_e - \mathbf{d}_e^{\mathrm{T}} \mathbf{g}_e + \mathbf{c}_e^{\mathrm{T}} \mathbf{G}_e \mathbf{d}_e \tag{26}$$

in which

$$\left[\mathbf{H}_e = \textstyle\int_{\Gamma_e} \mathbf{Q}_e^{\mathrm{T}} \mathbf{N}_e \mathrm{d}\Gamma \ \mathbf{G}_e = \textstyle\int_{\Gamma_e} \mathbf{Q}_e^{\mathrm{T}} \tilde{\mathbf{N}}_e \mathrm{d}\Gamma \ \mathbf{g}_e = \textstyle\int_{\Gamma_{te}} \tilde{\mathbf{N}}_e^{\mathrm{T}} \bar{t} \mathrm{d}\Gamma \right]$$

To enforce inter-element continuity on the common element boundary, the unknown vector $\mathbf{c}_e$ should be represented in terms of the nodal DOF $\mathbf{d}_e$. An optional relationship between $\mathbf{c}_e$ and $\mathbf{d}_e$ in the sense of variation can be obtained by minimization of the functional Π_e with respect to $\mathbf{c}_e$

$$\frac{\partial \Pi_e}{\partial \mathbf{c}_e^{\mathrm{T}}} = -\mathbf{H}_e\mathbf{c}_e + \mathbf{G}_e\mathbf{d}_e = \mathbf{0} \tag{27}$$

which leads to

$$\mathbf{c}_e = \mathbf{H}_e^{-1}\mathbf{G}_e\mathbf{d}_e \tag{28}$$

and then yields the expression Π_e only in terms of $\mathbf{d}_e$ and other known matrices

$$\Pi_e = \frac{1}{2}\mathbf{d}_e^{\mathrm{T}}\mathbf{G}_e^{T}\mathbf{H}_e^{-1}\mathbf{G}_e\mathbf{d}_e - \mathbf{d}_e^{\mathrm{T}}\mathbf{g}_e \tag{29}$$

Therefore, by taking the vanishing functional Π_e with respect to $\mathbf{d}_e$

$$\frac{\partial \Pi_e}{\partial \mathbf{d}_e^{\mathrm{T}}} = \mathbf{G}_e^{T}\mathbf{H}_e^{-1}\mathbf{G}_e\mathbf{d}_e - \mathbf{g}_e = \mathbf{0} \tag{30}$$

the stiffness equation can be expressed as

$$\mathbf{K}_e\mathbf{d}_e = \mathbf{g}_e \tag{31}$$

where $\mathbf{K}_e = \mathbf{G}_e^{\mathbf{T}}\mathbf{H}_e^{-1}\mathbf{G}_e$ stands for the element stiffness matrix.

It is worth noting that the evaluation of the right-hand vector $\mathbf{g}_e$ in Eq. (31) is the same as that in conventional FEM, which is obviously convenient for the implementation of HGS-FEM into existing FEM programs.

2.5 Recovery of rigid-body motion

Similar to the HT-FEM and HFS-FEM, it is necessary to recover the missing rigid-body motion modes from the above results in the proposed HGS-FEM.

Following the method presented by [Qin (2000)], the missing rigid-body motion can be recovered by writing the internal potential field of a particular element e as

$$u_e = \mathbf{N}_e\mathbf{c}_e + c_0 \tag{32}$$

where the undetermined rigid-body motion parameter c_0 can be calculated using the least square matching of u_e and $\tilde{u}_e$ at element nodes

$$\sum_{i=1}^{n} \left(\mathbf{N}_e\mathbf{c}_e + c_0 - \tilde{u}_e\right)^2\Big|_{\text{node } i} = \min \tag{33}$$

which finally gives

$$c_0 = \frac{1}{n}\sum_{i=1}^{n} \Delta u_{ei} \tag{34}$$

in which $\Delta u_{ei} = (\tilde{u}_e - \mathbf{N}_e\mathbf{c}_e)|_{\text{node } i}$ and n is the number of element nodes.

Once the nodal field is determined by solving the final stiffness equation, the coefficient vector $\mathbf{c}_e$ can be evaluated from Eq. (31), and then c_0 is evaluated from Eq. (34). Finally, the potential field u at any internal point in an element can be obtained by means of Eq. (32).

3 Numerical results and discussions

In this section, the efficiency, accuracy and convergence of the HGS-FEM are assessed by considering three numerical examples. The performance of the proposed method is assessed by comparing the present results with those from HFS-FEM with different fictitious parameters, boundary knot method (BKM) and analytical solution. To provide a more quantitative understanding of the results, the average relative error Rerr(u), Rerrx(t_x) and Rerry(t_y) defined, respectively, by

$$Rerr(u) = \sqrt{\frac{1}{NT}\sum_{i=1}^{NT}\left|\frac{u(i)-\bar{u}(i)}{\bar{u}(i)}\right|^2}, \tag{35a}$$

$$Rerrx(t_x) = \sqrt{\frac{1}{NT}\sum_{i=1}^{NT}\left|\frac{t_x(i)-\bar{t}_x(i)}{\bar{t}_x(i)}\right|^2}, \tag{35b}$$

$$Rerry(t_y) = \sqrt{\frac{1}{NT}\sum_{i=1}^{NT}\left|\frac{t_y(i)-\bar{t}_y(i)}{\bar{t}_y(i)}\right|^2}, \tag{35c}$$

are employed in numerical analysis, where $t = t_x n_{x_1} + t_y n_{x_2}$ and $\bar{t} = \bar{t}_x n_{x_1} + \bar{t}_y n_{x_2}$, $\bar{u}(i)$, $\bar{t}_x(i)$ and $\bar{t}_y(i)$ are the analytical solutions at x_i, and $u(i)$, $t_x(i)$ and $t_y(i)$ the related numerical solutions at $x_{i,}$ respectively. NT denotes the total number of uniform test points in the domain of interest. In addition, unless otherwise specified, the number of source points in intra-element field is equal to number of interpolation nodes in frame field, namely, $Ns = Nf$ in all the following numerical comparisons.

Example 1: First we verify the accuracy of the proposed formulation and investigate the effect of different nodes in an element on the accuracy displayed in Fig.1. Consider 2D homogeneous Helmholtz problem$\left(\Delta+\lambda^2\right)u = 0$in a square domain subjected to mixed boundary condition (Fig. 2a), where wave number$\lambda = \sqrt{2}$.

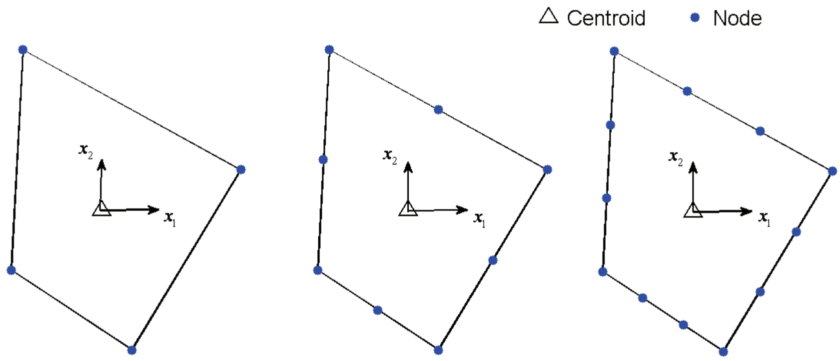

Figure 1: Configuration of different number of nodes in an element (Nf=4,8,12) used in the proposed HGS-FEM method

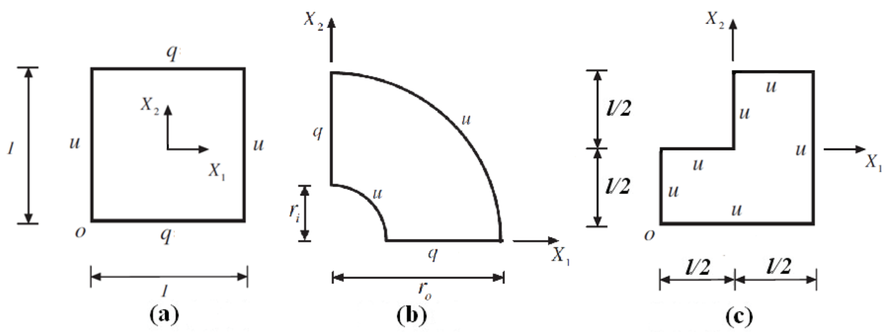

Figure 2: Configuration of different physical domains in this study

The analytical solution is $u = \sin(x_1)\cos(x_2)$, the corresponding mixed boundary conditions can be easily derived from the analytical solution.

Fig. 3a displays the condition number of stiffness matrix K in example 1 with respect to the number of elements by using the proposed HGS-FEM with different number of nodes in an element as shown in Fig 1. Figs. 3b-d show the numerical accuracy of temperature and heat flux varies against the number of elements from the proposed method with different number element nodes. Condition number *Cond* in Fig 3a is defined as the ratio of the largest and smallest singular value. It should be mentioned that, in general, the increasing node number in a particular element in the proposed method can improve the numerical accuracy; however, the accuracy with 12-node element becomes worse along with refinement of the

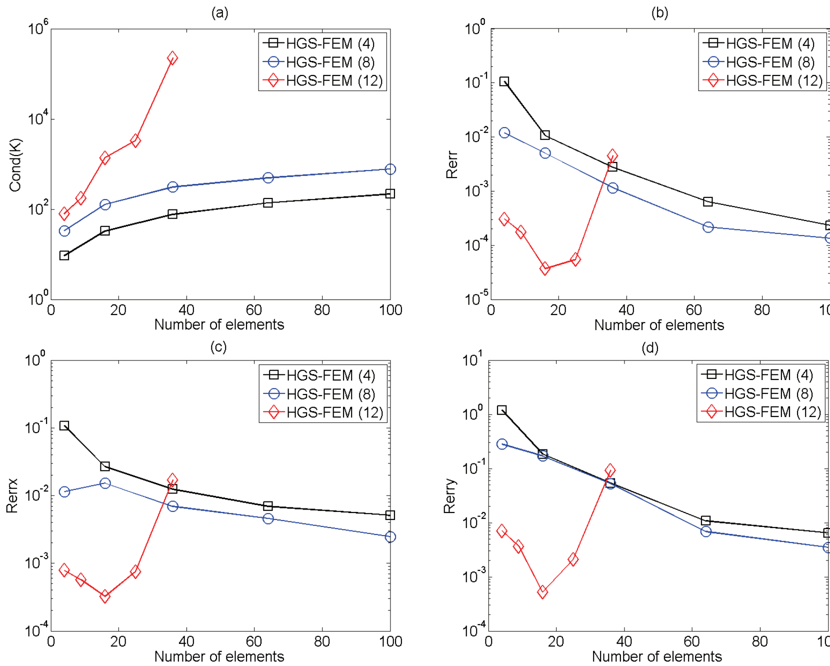

Figure 3: (a)The condition number of the interpolation matrix, and accuracy variation of (b) temperature, heat flux in (c) x_1 and (d)x_2 directions of example 1 against the number of elements by HGS-FEM with different-nodes elements (4,8,12)

element meshes due to the rapid increase of condition number. Therefore, the 8-node element is the suitable choice in the proposed HGS-FEM. Unless otherwise specified, we use the proposed HGS-FEM with 8-node element in all the following numerical assessments.

Example 2: This example compares the present method with HFS-FEM in 2D modified Helmholtz problem $\left(\Delta - \lambda^2\right) u = 0$, where $\lambda = \sqrt{2}$. The physical domain is formed from a quarter annulus with an outer radius $r_o = 10$ and an inner radius $r_i = 5$ (Fig. 2b). The analytical solution is $u = e^{x_1+x_2}$, the corresponding mixed boundary conditions also can be easily derived from the analytical solution.

Fig. 4a plots the condition numbers from the proposed method and HFS-FEM with different fictitious boundary parameter $d = 4, 6, 10$ varying against the element number, where d characterizes the distance between the fictitious and real boundaries. It can be observed from Fig. 4a, that both these two schemes above have similar trends that condition number increases along with an increase in the el-

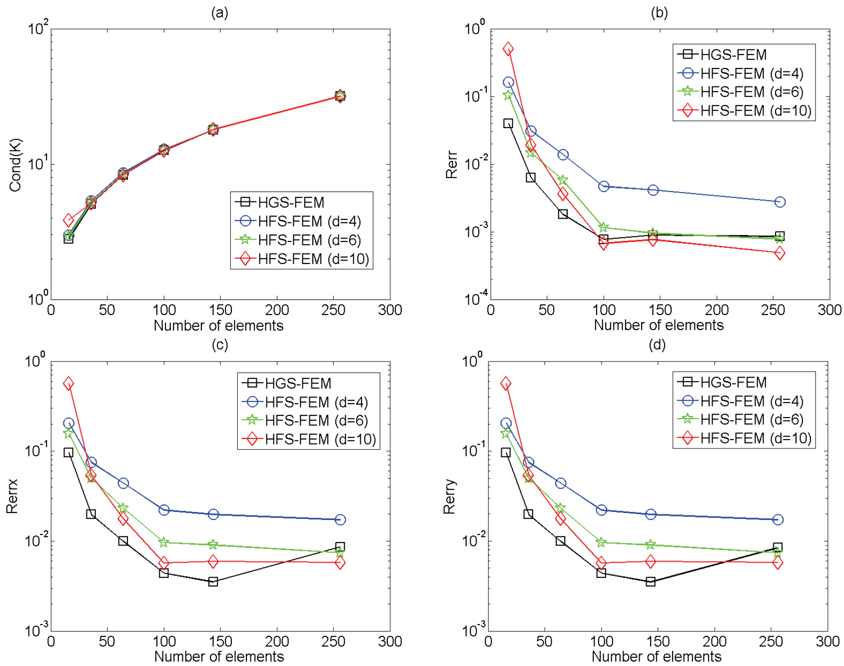

Figure 4: (a)The condition number of the interpolation matrix, and accuracy of (b) temperature and heat flux in (c) x_1 and (d)x_2 directions of example 2 vary against the number of elements by HGS-FEM and HFS-FEM with different fictitious boundary parameters (d=4,6,10)

ement number. Figs. 4b-d present the convergent rate of temperature and heat flow from the proposed method and HFS-FEM with *d=4,6,10* against with the number of elements. It can be seen from these figures that the proposed method behaviors better than HFS-FEM when the number of elements is less than 150, and the parameter d in HFS-FEM has a remarkable influence on numerical accuracy, In general, the larger parameter $d$provides the more accurate results, however, the results from HFS-FEM is unstable when $d = 10$ and the number of elements is less than 50. Moreover, it should be mentioned that the solution may not be correct by using HFS-FEM with $d = 2$. Therefore, it can be concluded that the fictitious boundary parameter d in HFS-FEM is a problem-dependent parameter, and still quite tricky and often troublesome to select it appropriately. Therefore, the proposed method has the advantage over the HFS-FEM in that no fictitious boundary is required at all.

Example 3: Consider 2D heat conduction problem $\sum\limits_{i,j=1}^{2} \frac{\partial}{\partial x_i}\left(K_{ij}(x,T)\frac{\partial u(x)}{\partial x_j}\right) = 0$ in a L-shape FGM (Fig 2c) with nonlinear thermal conductivity $K_{ij}(x,T) = a(T)\bar{K}_{ij}e^{\sum\limits_{i=1}^{2} 2\beta_i x_i}$, where $a(T) = 1+\frac{T}{2}, (\bar{K}_{ij}) = \begin{pmatrix} 2 & 0 \\ 0 & 1 \end{pmatrix}$, $\beta_1 = 0,\ \beta_2 = 1$. The tested solution [Marin and Lesnic (2007)] is

$$u(x) = -2+2\sqrt{1+T(x)} \tag{36}$$

in which

$$T(x) = \sqrt{\frac{1-Tx/Tr}{2Tr}}\sinh(Tr)e^{-Ty} \tag{37}$$

where $Tx = \frac{x_1}{\sqrt{2}} - 1,\ Ty = x_2,\ Tr = \sqrt{Tx^2+Ty^2}$. The corresponding Dirichlet boundary conditions also can be easily derived from the analytical solution.

By implementing the Kirchhoff transformation in conjunction with various variable transformations, the original governing equation transforms into the following Helmholtz-type equation

$$\left(\sum_{i,j=1}^{2}\left(\bar{K}_{ij}\frac{\partial^2 T(x)}{\partial x_i \partial x_j} + 2\beta_i \bar{K}_{ij}\frac{\partial T(x)}{\partial x_j}\right)\right)e^{\sum\limits_{i=1}^{2} 2\beta_i x_i} = 0,\ x \in \Omega \tag{38}$$

The corresponding nonsingular general solution [Fu et al. (2011)] of Eq.(38) is

$$u_G(x,y) = -\frac{I_0(\lambda R_G)}{2\pi\sqrt{\Delta_{\bar{K}}}}e^{-\sum\limits_{i=1}^{2}\beta_i(x_i+y_i)} \tag{39}$$

in which $\Delta_{\bar{K}} = \det(\bar{K}) = \bar{K}_{11}\bar{K}_{22} - \bar{K}_{12}^2 > 0, R_G = \sqrt{\sum\limits_{i=1}^{2}\sum\limits_{j=1}^{2} r_i \bar{K}_{ij}^{-1} r_j}, r_1 = x_1 - y_1, r_2 = x_2 - y_2$, where x, y are collocation points and source points, respectively, and I_0 denotes the zero-order modified Bessel function of first kind. The more details about this derivation can be found in Appendix 2.

We compare the proposed method with boundary knot method in this case. Numerical results of example 3 by the proposed HGS-FEM are displayed in Table 1. Table 2 shows the result obtained by BKM. It can be observed from Table 1 that the proposed method can provide acceptable numerical accuracy with only 3 elements. Furthermore, the HGS-FEM converges obviously to the analytical solution when increasing mesh density up to a critical value (108 in this example). But the increase of convergence rate slowdown slowly when approaching the critical and even diverging when the element number is greater than the critical value due to the ill condition of matrix H_e. From Table 2, it can be found that the numerical accuracy has less improvement through increasing boundary knots due to the large BKM condition number. Having compared the convergent performance of these two methods, it can be concluded that the HGS-FEM has the similar accuracy with that from BKM when the number of knots in less than 60, and becomes more accurate than BKM when the knot number is greater than 60.

4 Conclusions

In this paper, we apply a new type of nonsingular general solution as an interior trial function in the hybrid finite element model (HGS-FEM). The present scheme inherits the advantages of the HT-FEM over the conventional FEM and BEM, and removes the difficulty in constructing and choosing appropriate terms of Trefftz functions used in the HT-FEM, and the difficulty for determining the fictitious boundary used in the HFS-FEM. Numerical demonstration shows that the proposed HGS-FEM is a competitive numerical method for solving engineering problems. In comparison with HFS-FEM and BKM, the HGS-FEM performs more accurately and stably, and converges faster to analytical solution. Furthermore, the proposed method can be easily extended to other engineering problems by employing the corresponding general solution and constructing the related variational functional, and it is also easily combined with dual reciprocity technique [Partridge et al. (1992)] and multiple reciprocity technique [Fu and Chen (2009); Nowak and Neves (1994)] for solving inhomogeneous and nonlinear problems. This work is under way.

Acknowledgement: The work described in this paper was supported by the National Basic Research Program of China (973 Project No. 2010CB832702) and Fundamental Research Funds for the Central Universities (Grant No. 2010B15214). The first author would also like to thank the China Scholarship Council (CSC) for the financial support.

Appendix 1

The nonsingular general solutions to commonly used differential operators are listed in Table 3. In the table, Δ denotes Laplacian, ∇ the gradient operator, D the diffusivity coefficient, λ a real number known as the wave number, $\mathbf{v}$ and $\mathbf{r}$ are the velocity vector and distance vector, $\mu = \left(\left(\frac{|\mathbf{v}|}{2D} \right)^2 + \frac{\lambda}{D} \right)^{\frac{1}{2}}$ and r the Euclidean norm between the point x and the origin. Furthermore, I_0 and J_0 are the Bessel and

Table 1: Numerical results of Example 3 by HGS-FEM with different numbers of elements (knots)

Method	HGS-FEM					
Element (Knots)	3 (18)	12 (53)	27 (106)	48 (177)	75 (266)	108 (373)
Cond(K)	1.8702	6.3935	14.8539	26.1396	208.089	867.317
Cond(H_e)	6.397e+15	2.249e+16	1.996e+16	3.950e+16	3.304e+16	1.947e+17
Rerr	6.371 e-3	1.072 e-3	3.621 e-4	1.104 e-4	7.432 e-5	5.375 e-5
Rerrx	6.249 e-2	1.794 e-2	9.142 e-3	4.841 e-3	2.929 e-3	2.533 e-3
Rerry	5.059 e-2	1.270 e-2	8.970 e-3	3.827 e-3	3.066 e-3	3.440 e-3

Table 2: Numerical results of Example 3 by BKM with different numbers of boundary knots

Method	BKM					
Knots	16	56	104	176	256	376
Cond(K)	5.809e+17	2.052e+19	2.822e+20	1.976e+19	3.707e+19	1.160e+20
Rerr	4.104 e-3	6.315 e-3	2.353 e-3	2.270 e-3	2.215 e-3	6.712 e-2
Rerrx	5.237 e-2	1.747 e-2	2.246 e-2	2.090 e-2	2.074 e-2	8.077 e-2
Rerry	1.040 e-1	3.181 e-2	6.361 e-2	5.921 e-2	5.794 e-2	1.069 e-1

Table 3: Nonsingular general solutions to commonly used differential operators.

$\Re$	2D	3D
$\Delta+\lambda^2$	$\frac{1}{2\pi}J_0(\lambda r)$	$\frac{\sin(\lambda r)}{4\pi r}$
$\Delta-\lambda^2$	$\frac{1}{2\pi}I_0(\lambda r)$	$\frac{\sinh(\lambda r)}{4\pi r}$
$D\Delta+\mathbf{v}\bullet\nabla-\lambda^2$	$\frac{1}{2\pi}I_0(\mu r)e^{-\frac{\mathbf{v}\bullet\mathbf{r}}{2D}}$	$\frac{\sinh(\mu r)}{4\pi r}e^{-\frac{\mathbf{v}\bullet\mathbf{r}}{2D}}$

modified Bessel functions of the first kind of order zero.

Appendix 2

Consider the heat conduction problem in example 3

$$\sum_{i,j=1}^{2}\frac{\partial}{\partial x_i}\left(K_{ij}(x,T)\frac{\partial T(x)}{\partial x_j}\right)=0,\ x\in\Omega \tag{A1}$$

with the boundary conditions:
Dirichlet/Essential condition

$$T(x)=\bar{T},\quad x\in\Gamma_D \tag{A2a}$$

Neumann/Natural condition

$$q(x)=-\sum_{i,j=1}^{2}K_{ij}\frac{\partial T(x)}{\partial x_j}n_i(x)=\bar{q},\quad x\in\Gamma_N \tag{A2b}$$

Robin/Convective condition

$$q(x)=h_e(T(x)-T_\infty),\quad x\in\Gamma_R \tag{A2c}$$

By employing the Kirchhoff transformation

$$\varphi(T)=\int a(T)dT \tag{A3}$$

Eqs. (A1) and (A2) can be reduced as the following form

$$\left(\sum_{i,j=1}^{2}\left(\bar{K}_{ij}\frac{\partial^2\Phi_T(x)}{\partial x_i\partial x_j}+2\beta_i\bar{K}_{ij}\frac{\partial\Phi_T(x)}{\partial x_j}\right)\right)e^{\sum\limits_{i=1}^{2}2\beta_i x_i}=0,\ x\in\Omega \tag{A4}$$

$$\Phi_T(x)=\varphi(\bar{T}),\ x\in\Gamma_D \tag{A5a}$$

$$q(x) = -\sum_{i,j=1}^{2} K_{ij} \frac{\partial T(x)}{\partial x_j} n_i(x) = -e^{\sum_{i=1}^{2} 2\beta_i x_i} \sum_{i,j=1}^{2} \bar{K}_{ij} \frac{\partial \Phi_T(x)}{\partial x_j} n_i(x) = \bar{q}, \quad x \in \Gamma_N \tag{A5b}$$

$$q(x) = h_e\left(\Phi_T(x) - \phi\left(T_\infty\right)\right), \quad x \in \Gamma_R \tag{A5c}$$

where $\Phi_T(x) = \phi(T(x))$and the inverse Kirchhoff transformation

$$T(x) = \phi^{-1}\left(\Phi_T(x)\right) \tag{A6}$$

And then we derive the nonsingular general solution of Eq. (A4) by two-step variable transformations:

Step1: To simplify the expression of Eqs. (A4), let $\Phi_T = \Psi e^{-\sum_{i=1}^{2} \beta_i (x_i + s_i)}$. Eqs. (A4) can then be rewritten as follows:

$$\left(\sum_{i,j=1}^{2} \bar{K}_{ij} \frac{\partial \Psi(x)}{\partial x_i \partial x_j} - \lambda^2 \Psi(x)\right) e^{\sum_{i=1}^{2} \beta_i (x_i + s_i)} = 0, \; x \in \Omega \tag{A7}$$

where $\lambda = \sqrt{\sum_{i=1}^{2} \sum_{j=1}^{2} \beta_i \bar{K}_{ij} \beta_j}$. Since $e^{\sum_{i=1}^{2} \beta_i (x_i + s_i)} > 0$. The Trefftz functions of Eq. (A7) are equal to those of anisotropic modified Helmholtz equation.

Step2: To transform the anisotropic equation (A7) into isotropic one, we set

$$\begin{pmatrix} y_1 \\ y_2 \end{pmatrix} = \begin{pmatrix} 1/\sqrt{\bar{K}_{11}} & 0 \\ -\bar{K}_{12}/\sqrt{\bar{K}_{11}\Delta_{\bar{K}}} & \sqrt{\bar{K}_{11}}/\sqrt{\Delta_{\bar{K}}} \end{pmatrix} \begin{pmatrix} x_1 \\ x_2 \end{pmatrix} \tag{A8}$$

where $\Delta_{\bar{K}} = \det(\bar{K}) = \bar{K}_{11}\bar{K}_{22} - \bar{K}_{12}^2 > 0$.
It follows from Eq. (A7) that

$$\left(\sum_{i=1}^{2} \frac{\partial^2 \Psi(y)}{\partial y_i \partial y_i} - \lambda^2 \Psi(y)\right) = 0, \; y \in \Omega \tag{A9}$$

Therefore, Eq. (A9) is the isotropic modified Helmholtz equation, the corresponding nonsingular solution can be found in [Chen and Tanaka (2002)]. Then the nonsingular solution of Eq. (A7) can be obtained by using inverse transformation (A8),

$$u_G(x,s) = -\frac{1}{2\pi\sqrt{\Delta_{\bar{K}}}} I_0(\lambda R) \tag{A10}$$

in which $R = \sqrt{\sum_{i=1}^{2}\sum_{j=1}^{2} r_i \bar{K}_{ij}^{-1} r_j}, r_1 = x_1 - s_1, r_2 = x_2 - s_2$, where x, s are collocation points and source points, respectively, and I_0 denotes the zero-order modified Bessel function of first kind.

Finally, by implementing the variable transformation $\Phi_T = \Psi e^{-\sum_{i=1}^{2}\beta_i(x_i+s_i)}$, the non-singular solution of Eq. (A4) is in the following form

$$u_G(x,s) = -\frac{I_0(\lambda R)}{2\pi\sqrt{\Delta_{\bar{K}}}} e^{-\sum_{i=1}^{2}\beta_i(x_i+s_i)} \tag{A11}$$

References

Atluri, SN. (1971): An Assumed Stress Hybrid Finite Element Model for Linear elastodynamic Analysis *AIAA Journal*,vol. 11(7), pp. 1028-1031.

Atluri, SN. (1973): On the Hybrid Stress Finite Element Model for Incremental Analysis of Large Deflection Problems *International Journal of Solids and Structures*,vol. 1, pp. 1177-1191.

Atluri, SN; Chen, WH; Nakagaki, M; Kathiresan, K; Rhee, HC. (1978): Hybrid finite element models for linear and nonlinear fracture analyses Numerical methods in fracture mechanics, Luxmoore AR,Owen DRJ, eds., Swansea, United Kingdom, pp. 52-66.

Atluri, SN; Kobayashi, AS; Nakagaki, M. (1975): An Assumed Displacement Hybrid Finite Element Model for Linear Fracture Mechanics *International Journal of Fracture*,vol. 11(2), pp. 257-271.

Chen, W; Fu, ZJ; Jin, BT. (2010): A truly boundary-only meshfree method for inhomogeneous problems based on recursive composite multiple reciprocity technique. *Engineering Analysis with Boundary Elements*,vol. 34(3), pp. 196-205.

Chen, W; Shen, ZJ; Shen, LJ; Yuan, GW. (2005): General solutions and fundamental solutions of varied orders to the vibrational thin, the Berger, and the Winkler plates. *Engineering Analysis with Boundary Elements*,vol. 29(7), pp. 699-702.

Chen, W; Tanaka, M. (2002): A meshless, integration-free, and boundary-only RBF technique. *Computers & Mathematics with Applications*,vol. 43(3-5), pp. 379-391.

Dhanasekar, M; Han, JJ; Qin, QH. (2006): A hybrid-Trefftz element containing an elliptic hole. *Finite Elements in Analysis and Design*,vol. 42(14-15), pp. 1314-1323.

Fairweather, G; Karageorghis, A. (1998): The method of fundamental solutions for elliptic boundary value problems. *Advances in Computational Mathematics*,vol. 9(1-2), pp. 69-95.

Fu, ZJ; Chen, W. (2009): A Truly Boundary-Only Meshfree Method Applied to Kirchhoff Plate Bending Problems. *Advances in Applied Mathematics and Mechanics*,vol. 1(3), pp. 341-352.

Fu, ZJ; Chen, W; Qin, QH. (2011): Boundary Knot Method for Heat conduction in nonlinear functionally graded material. *Engineering Analysis with Boundary Elements*,vol. 35(5), pp. 729-734.

Jirousek, J; Leon, N. (1977): A powerful finite element for plate bending. *Computer Methods in Applied Mechanics and Engineering*,vol. 12(1), pp. 77-96.

Marin, L; Lesnic, D. (2007): The method of fundamental solutions for nonlinear functionally graded materials. *International Journal of Solids and Structures*,vol. 44(21), pp. 6878-6890.

Nowak, AJ; Neves, AC. (1994): *The Multiple Reciprocity Boundary Element Method.* Computational Mechanics Publication.

Partridge, PW; Brebbia, CA; Wroble, LC. (1992): *The dual reciprocity boundary element method* Computational Mechanics Publications.

Pian, THH. (1964): Derivation of element stiffness matrices by assumed stress distributions. *AIAA Journal*,vol. 2, pp. 1333-1336.

Pian, THH. (1983): Reflections and remarks on hybrid and mixed finite element methods. Hybrid and Mixed Finite Element Method, Atluri SN, Gallagher RH,Zienkiewicz OC, eds., Wiley Kc Sons, New York, pp. 565.

Pian, THH. (1995): State-of-the-art development of hybrid/mixed finite element method. *Finite Elements in Analysis and Design*,vol. 21(1-2), pp. 5-20.

Pian, THH; Tong, P. (1969): Basis of finite element methods for solid continua. *International Journal for Numerical Methods in Engineering*,vol. 1(1), pp. 3-28.

Piltner, R. (1985): Special finite elements with holes and internal cracks. *International Journal for Numerical Methods in Engineering*,vol. 21(8), pp. 1471-1485.

Qin, QH. (1993): Nonlinear analysis of Reissner plates on an elastic foundation by the BEM. *International Journal of Solids and Structures*,vol. 30(22), pp. 2101-3111.

Qin, QH. (1994): Hybrid Trefftz Finite-Element Approach for Plate-Bending on an Elastic-Foundation. *Applied Mathematical Modelling*,vol. 18(6), pp. 334-339.

Qin, QH. (2000): *The Trefftz Finite and Boundary Element Method.* WIT Press, Southampton.

Qin, QH. (2003a): Solving anti-plane problems of piezoelectric materials by the

Trefftz finite element approach. *Computational Mechanics*,vol. 31(6), pp. 461-468.

Qin, QH. (2003b): Variational formulations for TFEM of piezoelectricity. *International Journal of Solids and Structures*,vol. 40(23), pp. 6335-6346.

Qin, QH. (2005): Trefftz Finite Element Method and Its Applications. *Applied Mechanics Reviews*,vol. 58(5), pp. 316-337.

Qin, QH; Wang, H. (2009): *Matlab and C Programming for Trefftz Finite Element Methods*. CRC Press, Boca Raton.

Simpson, HC; Spector, SJ. (1987): On the positivity of the second variation in finite elasticity. *Archive for Rational Mechanics and Analysis*,vol. 98(1), pp. 1-30.

Sladek, V; Sladek, J. (1998): *Singular Integrals in boundary element methods*. Computational Mechanics Publications, Southampton.

Tong, P. (1977): A hybrid crack element for rectilinear anisotropic material. *International Journal for Numerical Methods in Engineering*,vol. 11(2), pp. 377-382.

Tong, P; Pian, THH; Lasry, SJ. (1973): A hybrid-element approach to crack problems in plane elasticity. *International Journal for Numerical Methods in Engineering*,vol. 7(3), pp. 297-308.

Wang, H; Qin, QH. (2006): A meshless method for generalized linear or nonlinear Poisson-type problems. *Engineering Analysis with Boundary Elements*,vol. 30, pp. 515-521.

Wang, H; Qin, QH. (2009): Hybrid FEM with fundamental solutions as trial functions for heat conduction simulation. *Acta Mechanica Solida Sinica*,vol. 22(5), pp. 487-498.

Wang, H; Qin, QH. (2010): Fundamental-solution-based finite element model for plane orthotropic elastic bodies. *European Journal of Mechanics a-Solids*,vol. 29(5), pp. 801-809.

Xiao, QZ; Karihaloo, BL. (2007): An overview of a hybrid crack element and determination of its complete displacement field. *Engineering Fracture Mechanics*,vol. 74(7), pp. 1107-1117.

Ying, LA; Atluri, SN. (1983): A hybrid finite element method for stokes flow: Part II–Stability and convergence studies. *Computer Methods in Applied Mechanics and Engineering*,vol. 36(1), pp. 39-60.